Robotica (2025), **43**, pp. 2459–2479
doi:10.1017/S0263574725000499

CAMBRIDGE UNIVERSITY PRESS

RESEARCH ARTICLE

Experimental research of wheel-legged robot crossing obstacles

Xin Mei[1], Yongle Wei[2], Chenguang Guo[1] and Xingyuan Zhang[1]

[1]School of Mechanical Engineering, Liaoning Technical University, Fuxin, Liaoning, China
[2]College of Mechanical Engineering, Quzhou University, Quzhou, Zhejiang, China
Corresponding author: Yongle Wei; Email: weiyongle126@126.com

Received: 29 January 2024; **Revised:** 21 February 2025; **Accepted:** 13 March 2025; **First published online:** 24 June 2025

Keywords: wheel-legged robot; obstacle-crossing gait planning; mode switch

Abstract

Wheel-leg composite robots exhibit robust mobility and exceptional obstacle-crossing capabilities in complex environments. This paper proposes a novel transformable wheel-leg composite structure and presents the design of a wheel-leg composite obstacle-crossing robot, fundamentally configured as a two-wheeled quadruped. The research encompasses a comprehensive analysis of the robot's overall mechanical structure, a detailed kinematic investigation of its body and obstacle-crossing gait planning, virtual prototype dynamics simulation, and field experimentation. Utilizing advanced modeling software, a 3D model of the robot was established. The kinematic characteristics of the robot in both wheeled and legged modes were thoroughly examined. Specifically, for the legged mode, the Denavit-Hartenberg coordinate system was established, and a detailed kinematic model was analyzed. The obstacle-crossing gait was planned based on the robot's leg action mechanism. Furthermore, the Lagrangian method was employed to develop a mathematical model for the dynamics of the robot in both wheel-foot modes, allowing for a comprehensive force analysis. To validate the feasibility and rationality of the robot's obstacle-crossing capabilities under various conditions, extensive simulations and prototype tests were conducted across diverse terrains. The results provide valuable insights and practical guidance for the structural design of wheel-leg composite obstacle-crossing robots, contributing to advancements in this promising field.

1. Introduction

The transmission and transformation of mechanical motion constitutes the foundational element for realizing the fundamental functionalities of mobile robot mechanical systems. Furthermore, the mechanism serves as the structural backbone and executing components of these systems. Consequently, the essence of innovation within mechanical systems lies in the advancement of mechanisms [1]. Currently, robot locomotion mechanisms are primarily categorized into wheeled and legged varieties. Wheeled robots exhibit superior speed and stability on highly planar surfaces, yet their obstacle-crossing capabilities are limited. Conversely, legged robots demonstrate robust obstacle-crossing abilities and exceptional traversability in complex environments, albeit generally at slower speeds. Fusing the advantages of wheeled robots and legged robots, designing wheel-leg composite robots is a powerful initiative for mobile robot mechanism innovation [2]. Many scholars have proposed various excellent solutions to solve the problem of poor obstacle-crossing performance of wheeled mechanisms [3–7], and wheel-legged mobile robots with strong maneuverability and topology variation have been applied to various complex road conditions. Wheel-leg variable obstacle-crossing robots can not only maintain efficient mobility when dealing with flat road surfaces but also exert superior obstacle-crossing ability when encountering non-structured road surfaces. Mao Nan et al. [8] from King's College London and Southern University of Science and Technology designed a wheeled bipedal robot with a parallel five-bar linkage as the leg module, which is able to compensate for the tilt angle of the chassis through the

© The Author(s), 2025. Published by Cambridge University Press.

https://doi.org/10.1017/S0263574725000499 Published online by Cambridge University Press

basic principle of inverted pendulum, and can effectively reduce the need for additional mating. Erika Ottaviano and Pierluigi Rea et al. [9] at the University of Cassino and Southern Lazio have designed and built a leg-front wheel-legged robot using the mechanical principle of four-link transmission, which is able to perform turning and obstacle-crossing functions by means of a 2-degree-of-freedom wheel-legged walking robot prototype. Lining Sun et al. [10] In making sideline tilt judgments and recoveries by adjusting the optimal swing leg to the stance state, the mass distribution was able to enable the projection of the center of gravity to always be located in the region bounded by the ground contact point.

The walking wheel is used as a component module of the mobile robot body, and then the leg folding problem is investigated, professor Liang of Harbin Institute of Technology [11] has also developed a related multimodal robot. Cao et al. [12] from Taiyuan University of Technology designed a quadrupedal robot with wheel-leg separation, which achieves dynamic switching of wheel-leg modes through algorithmic control advantages. For example, in 2014, Yoo-Seok Kim et al. [13] of Seoul National University, South Korea, combined the advantages of the circular wheel and the leg wheel, using the foot and the rotating ankle joint to trigger the conversion into a leg and foot, three legs are enough to rotate and combine into a wheel with the axle as the center, and the hub of the wheel and the segmented legs are connected by spokes, and the basic idea is to segment the circular wheel into multiple legs, and each leg can rotate around a joint that corresponds to the end of the spoke axis. In 2018, Yang Yang et al., from Beijing University of Aeronautics and Astronautics [14], utilized a folding and spreading mechanism to achieve the transformation between wheel-type and wheel-leg-type configurations. Furthermore, they employed the intermediate trajectory of this mechanism to satisfy the deformation requirements of an extended-type configuration. Additionally, the researchers combined the wheel-type, extended-type, and wheel-legged configurations and proposed an optimization of the topology for the multi-segment deformation wheel. This optimization involved incorporating a specific length constraint relationship to meet the pertinent requirements. In 2017, Servt SOYGUDER and colleagues from the United States [15] introduced a novel paradigm of self-reconfigurable robots, which retains a central rotary axis. This robotic system transitions from an O-shaped wheel configuration to an S-shaped one via a connecting rod-driven extension mechanism, thereby accomplishing the metamorphosis from a wheeled to a legged form. Distinct from wheel-leg folding mechanisms centered on the drive axis, a fresh wheel-leg hybrid robotic architecture was proposed by Kenshiro Tada et al. from Osaka University, Japan, in 2010 [16]. This design enables the formation of a larger wheel diameter, with its linear unfolding configuration strategically incorporating a three-part split in the original circular wheel diameter to enhance obstacle-crossing capability through articulation. Typically, such robots are equipped with multiple evenly distributed foldable short legs on the wheels. Through the rotation of the traveling wheels, each short leg sequentially engages with the ground, facilitating walking and obstacle navigation.

In this paper, we present the design of a Wheel-Legged Composite Robot (WLCR), a unique two-wheeled quadruped robot that incorporates transformable wheels. The main contributions of this paper are as follows. Section 2 introduces the novel design of a wheel-leg combination robot. It details the planning of the robot's wheel-to-leg transformation and walking gait, which are integral to its operational principle. Additionally, a center of mass adjustment mechanism is incorporated into the robot's framework to enhance its walking stability. Furthermore, this section establishes a theoretical framework for the robot's kinematics in both wheeled and legged states, outlining the principles underlying its obstacle-crossing capabilities. Section 3 delves into the dynamic analysis of the robot. Utilizing virtual prototype dynamics simulation technology, it focuses on the motion state of the WLCR during the obstacle-crossing process. This analysis provides a solid theoretical foundation for the development of an equilibrium motion control model for the robot during its walking process. Section 4 describes the fabrication of an equal-scale prototype based on the theoretical simulation model. The robot's electronic control system is further refined through debugging. Relevant experiments are conducted on various terrains, including flat ground and steps. During these experiments, force data from the robot's foot end while climbing steps are collected. The results, validated through a series of rigorous experimental processes, demonstrate that the designed WLCR exhibits significant terrain adaptability. This finding offers

https://doi.org/10.1017/S0263574725000499 Published online by Cambridge University Press

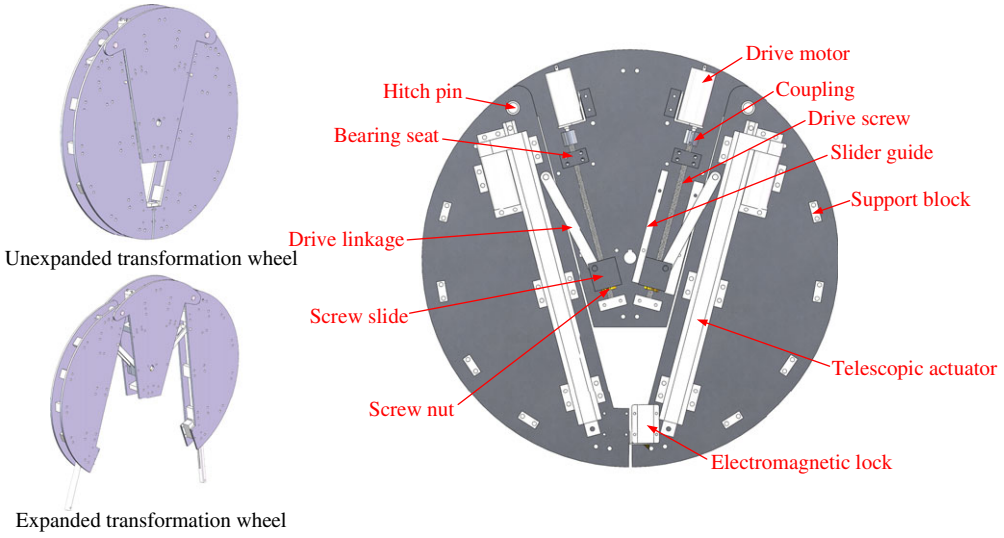


Figure 1. *Mechanical structure of transformable wheel.*

a fresh perspective for innovative design in traditional mechanical structures. Lastly, Section 5 concludes the paper.

2. Robot structure design and motion analysis

2.1. Transformer wheel configuration design

In this paper, we employ the methodology of a three-segment segmented circle to divide a solitary walking wheel into a stationary bracket and two oscillating legs. This approach enables the transition between wheel and leg configurations. The pivotal aspect of enabling gait walking for legged robots lies in dynamically adjusting the leg length during locomotion. Consequently, when the deformable wheel transitions into a leg-shaped structure, it necessitates a leg length adjustment mechanism to facilitate legged locomotion. Additionally, a leg pendulum actuation mechanism is indispensable. To mitigate the issue of excessive joint torque when driving directly around the leg pendulum's rotational axis, the leg pendulum actuation mechanism incorporates a linkage system to propel the deformable wheel structure, as illustrated in Figure 1.

Due to the characteristics of low-pair surface contact, the crank slider mechanism is capable of transmitting large amounts of power with minimal wear and tear, resulting in a longer lifespan. This is particularly important for robots that require prolonged, high-load operations. According to the principle of transformation wheel configuration, the leg length adjustment mechanism is realized by the telescopic push rod, and the leg swing drive mechanism is realized by the screw nut and connecting rod mechanism. The transformation wheel consists of bracket, swing leg, telescopic push rod, swing drive mechanism, leg swing drive mechanism consisting of screw nut vice, slider, transmission linkage, the movement of the two swing legs is driven by two sets of independent leg swing drive mechanism.

2.2. Robot overall structure

The two individual leg-pendulum drive mechanisms of the transformable wheel operate independently of each other, enabling a single transformable wheel to morph into two legs. Consequently, the chassis, in conjunction with two such transformable wheels, can be integrated to constitute a two-wheeled quadrupedal robot, as illustrated in Figure 2.

Two transformed wheels are symmetrically mounted on both lateral sides of the chassis, which comprises a structural frame, rolling drive motors, and a center-of-gravity adjustment mechanism. To ensure

https://doi.org/10.1017/S0263574725000499 Published online by Cambridge University Press

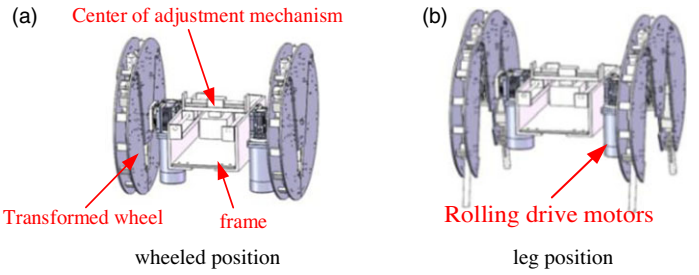


Figure 2. *Structures of wheel-legged robot.*

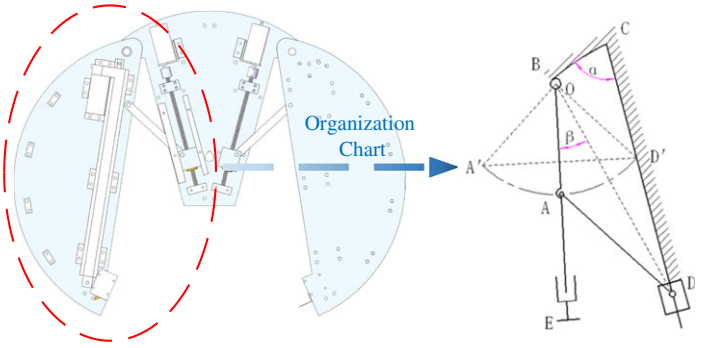


Figure 3. *Motion diagram of swinging-leg.*

the stability of the robot's two-wheeled rolling gait, the chassis's center of gravity is positioned beneath the rotational center of the transformed wheels. The center-of-mass adjustment mechanism, installed within the frame, serves to modify the robot's center of mass position for both wheeled and legged locomotion. Notably, the robot's power supply battery pack can function as a counterweight within this adjustment mechanism. The rolling drive motors, fixedly mounted on both sides of the frame, propel the transformed wheels, enabling the robot's wheeled mobility.

Upon transitioning the transformed wheels into a legged configuration, four sets of leg pendulum drive mechanisms are engaged to coordinate the synchronized movements of the four legs, thereby facilitating the robot's legged locomotion. In essence, after the transformation of the wheels into leg-like structures, these four legs are actuated by the respective sets of leg swing drive mechanisms to ensure coordinated motion, thereby enabling the robot to execute legged walking.

Due to the increased diameter of the transformed wheel, the robot exhibits enhanced efficiency when rolling on relatively flat surfaces and can readily traverse smaller gullies or obstacles. Furthermore, the extended stroke of the telescopic actuator equips the robot's legged mode with robust obstacle-crossing capabilities.

2.3. Swing leg motion analysis

Transformer wheels facilitate the conversion between wheeled and legged modes of locomotion. Specifically, when the robot adopts a legged gait using its legs and feet, the screw nut mechanism actuates the slider. This, in turn, through a connecting rod, drives the swinging leg to oscillate. A schematic illustration of the swinging leg's motion is depicted in Figure 3.

In order to avoid the singularity of the line AD coinciding with the articulation point O, resulting in the swing leg not being effectively deployed, the transformation wheel is in the wheel mode, the initial angle of the connecting rod $\angle DAE$ is approximately 14°, the point A, D are articulated. Connect the two points of OD, construct $\triangle AOD$ and $\triangle ODC$, and sort out the relationship between the angle of the swinging leg AO and the length of the moving vice of the screw nut in the process of swinging outward

https://doi.org/10.1017/S0263574725000499 Published online by Cambridge University Press

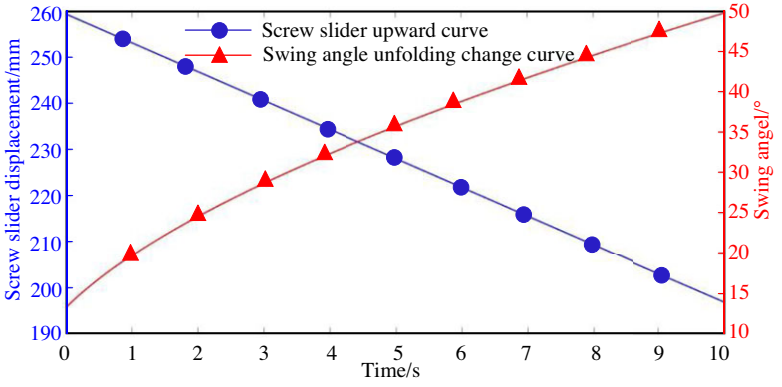


Figure 4. *Angle curve of swinging-leg.*

as follows:

$$\begin{cases} L_{OD}^2 = L_{CD}^2 + L_{OC}^2 - 2L_{CD} \cdot L_{OC} \cdot \cos\alpha \\ L_{AD}^2 = L_{AO}^2 + L_{OD}^2 - 2L_{AO} \cdot L_{OD} \cdot \cos\beta \end{cases} \tag{1}$$

Then,

$$\beta = \arccos\left[\frac{L_{AO}^2 + L_{CD}^2 + \mathrm{L}_{\mathrm{OC}}^2 - \mathrm{L}_{\mathrm{AD}}^2 - 2L_{CD} \cdot \mathrm{L}_{\mathrm{OC}} \cdot \cos\alpha}{2L_{AO} \cdot \sqrt{L_{CD}^2 + \mathrm{L}_{\mathrm{OC}}^2 - 2L_{CD} \cdot \mathrm{L}_{\mathrm{OC}} \cdot \cos\alpha}}\right] \tag{2}$$

where α indicates the fixed angle of the bracket,78.75°, β indicates the swing angle of the swing leg, L_{AO} indicates the radius of gyration of articulation point A,110 mm, L_{CD} indicates the length of the moving sub of the screw nut, L_{OC} indicates the length of the articulated arm of the bracket, 67.18 mm, L_{AD} indicates the length of the drive linkage,150 mm.

The length of the moving sub of the screw nut can be calculated from the slider moving speed and moving time:

$$L_{CD} = L_0 + vt \tag{3}$$

where L_0 indicates the initial distance of CD in the wheeled state, 259.38 mm, v denotes the speed of movement of slider D in the direction of CD, t indicates the moving time.

The slider traveling speed can be calculated from the motor speed and the screw pitch:

$$v = np \tag{4}$$

where n indicates the speed of the drive motor, p indicates the screw pitch used,1.25 mm.

The motion relationship expressed by Eqs. (2), (3), (4), written as a MATLAB program, and given the motor speed, can be calculated to obtain the swing leg swing angle, the screw nut moving sub-displacement, the curve of change with time as shown in Figure 4.

As can be seen from Figure 4, driven by the fixed speed of the motor, the slider moves at a constant speed, and the swinging angle curve of the swinging leg does not fluctuate sharply, indicating that the swinging leg movement process is smooth.

2.4. Robotic obstacle-crossing gait planning

When a two-wheeled quadrupedal robot traverses a flat surface or encounters minor obstacles, it employs a wheeled mode of locomotion, pressing over obstacles with relative ease. The motion sequence in this mode is straightforward: the two wheels rotate in unison, at the same speed, facilitating straightforward or backward linear movement, while differential wheel speeds induce turning. Conversely, when the robot transitions to legged locomotion or navigates significant obstacles, the motion sequence becomes

https://doi.org/10.1017/S0263574725000499 Published online by Cambridge University Press

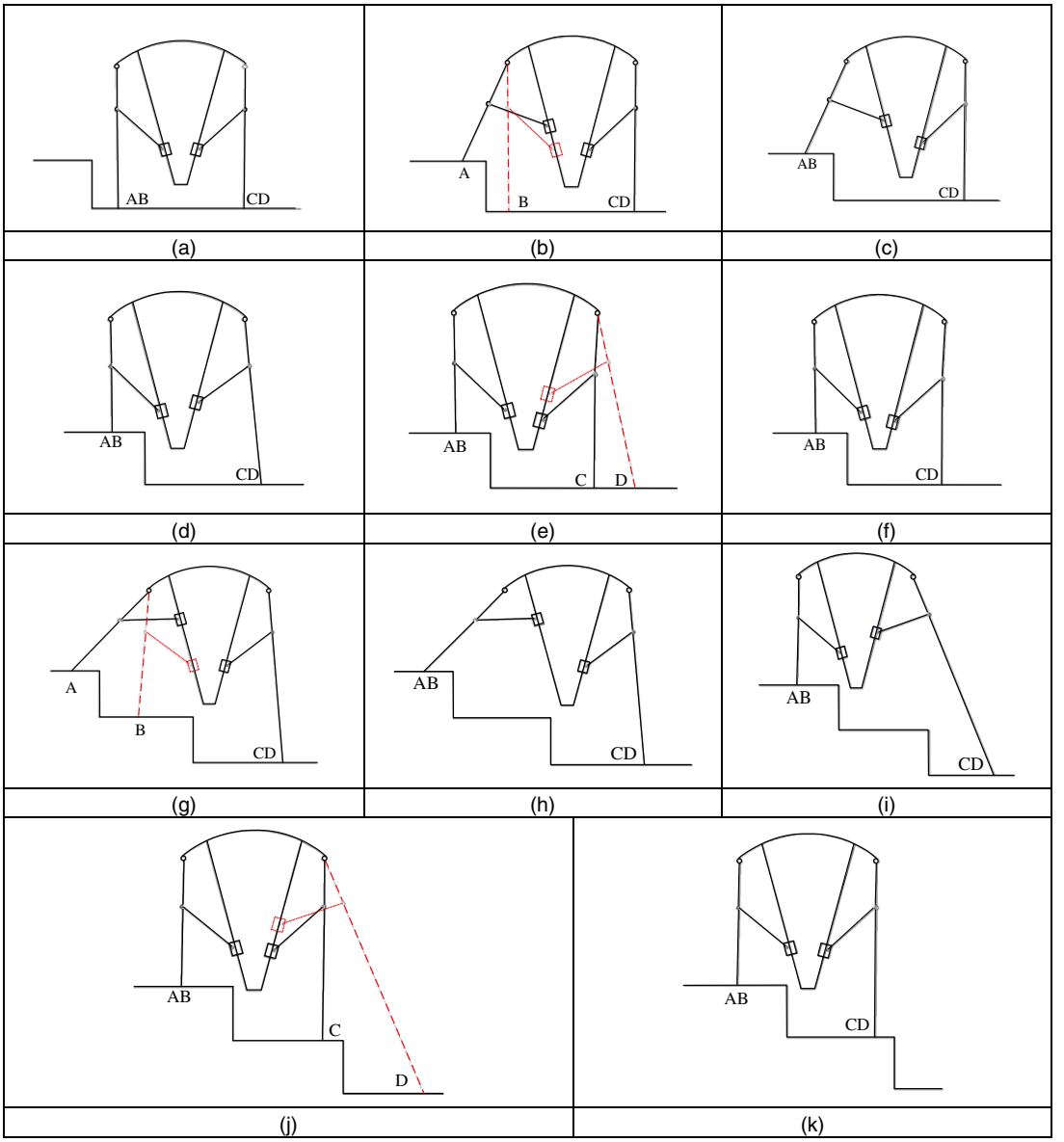


Figure 5. *Gait planning for robot crossing stair steps.*

more intricate. Considering a typical staircase obstacle as an illustrative example, the robot necessitates the planning of a gait sequence to successfully traverse the obstacle.

In general, a multi-legged robot typically employs three legs for supporting and propelling its body during locomotion, while the remaining legs function as swing legs [17].

The following example demonstrates the stair-climbing gait planning for a robot, as depicted in Figure 5. In this figure, the solid line represents the structural outline of the left-transformed wheel, whereas the dashed line corresponds to the structural outline of the right-transformed wheel. The foot ends of the left front leg, right front leg, left rear leg, and right rear leg are denoted by points A, B, C, and D, respectively. The sequence of the robot ascending a staircase step is detailed as follows.

https://doi.org/10.1017/S0263574725000499 Published online by Cambridge University Press

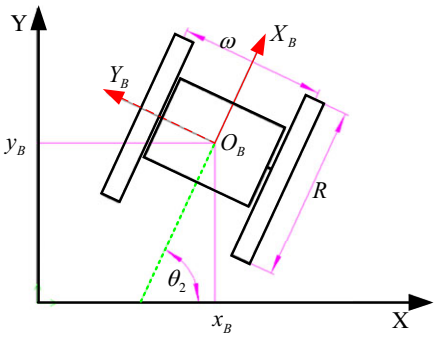


Figure 6. *Coordinate system for wheeled robot motion.*

(1) The robot advances to the front of the stairs via wheel-rolling or legged locomotion, adjusts to its initial posture, and prepares for the obstacle-crossing phase, as illustrated in Figure 5(a).

(2) The center-of-mass adjustment mechanism manipulates the counterweight block to the right rear of the robot. Simultaneously, the left front leg retracts, lifting off the ground and swinging forward to clear the first step. Subsequently, the left front leg extends once more until its foot end touches the ground at point A, as depicted in Figure 5(b).

(3) The center-of-mass adjustment mechanism positions the counterweight block to the left rear of the robot. Concurrently, the right front leg retracts, swings forward, and then extends until its foot terminally contacts the ground at point B, as illustrated in Figure 5(c).

(4) The center-of-mass adjustment mechanism displaces the counterweight block to the center of the robot. Subsequently, the four legs synchronously swing back, causing the center of mass of the robot to advance, as depicted in Figure 5(d).

(5) The center-of-mass adjustment mechanism repositions the counterweight block to the right front of the robot. Concurrently, the left hind leg retracts, swings forward, and extends until its foot reaches and contacts the ground at point C, as illustrated in Figure 5(e).

(6) The center-of-mass adjustment mechanism adjusts the position of the counterweight block to the left front of the robot. Subsequently, the right hind leg retracts, swings forward, and extends until its foot terminally contacts the ground at point D, as shown in Figure 5(f).

At this point, the robot's two front legs stand on the first step, and a set of obstacle-crossing action process is completed; cycling step (2) to step (6), the robot's front legs advance to the second step, while the back legs remain on the first step, as illustrated in Figure 5(g)–(k).

2.5. Robot motion analysis

2.5.1. Analysis of robotic wheeled motion

The left and right wheels of the robot use dual-drive differential steering to satisfy the conditions of pure rolling and no sliding in the lateral direction, the principle of self-balancing is like an inverted pendulum of the first order [18–19]. In the structured environment, the coordinate system of the robot's wheeled motion is established based on the top view of the two-dimensional plane as shown in the following Figure 6.

O is the origin of the global coordinate system, O_B is the origin of the local coordinate system of the robot, which is also the center of mass of the robot, X_B is along the forward direction of the robot, Y_B is perpendicular to the left side of the forward direction, ω is the angular velocity of the deformed wheel, and R is the diameter of the deformed wheel.

Based on the coordinate system shown in the above figure, the kinematic model of the differential drive-wheeled robot is obtained.

$$\begin{bmatrix} \ddot{x} \\ \ddot{y} \\ \ddot{\theta} \end{bmatrix} = \begin{bmatrix} \frac{R\cos\theta}{2} & \frac{R\cos\theta}{2} \\ \frac{R\sin\theta}{2} & \frac{R\sin\theta}{2} \\ \frac{-R}{v} & \frac{R}{v} \end{bmatrix} \begin{bmatrix} \omega_L \\ \omega_R \end{bmatrix} \tag{5}$$

https://doi.org/10.1017/S0263574725000499 Published online by Cambridge University Press

where y_B, x_B is a wheeled robot center of mass, O_B are the coordinates in the global coordinate system $\{0\}, \theta$ is the angle between the $X_B$axis and the OX axis in the global coordinate system, v denotes the speed of motion of the wheeled robot, R is the radius of the wheel of the robot, ω_L and ω_R are the angular velocities of the left and right transformed wheels respectively.

From the above formula, the motion information of the wheeled robot in the global coordinate system can be known if ω_L and ω_R are known.

In the working environment with high flatness, the position of the wheeled robot can be expressed by the robot's local coordinate system$\{O_B\}$, and the robot's trajectory speculative state equation is.

$$\begin{bmatrix} x_{i+1} \\ y_{i+1} \\ \theta_{i+1} \end{bmatrix} = \begin{bmatrix} x_i \\ y_i \\ \theta_i \end{bmatrix} + T \begin{bmatrix} \dot{x}_i \\ \dot{y}_i \\ \dot{\theta}_i \end{bmatrix} \tag{6}$$

where i denotes the ordinal number as a function of time, T is the interval between measurements.

Therefore, the trajectory speculation of the robot can be achieved by the derivation of the above equations about the motion state of the differential wheeled robot.

Meanwhile, in order to ensure that no lateral sliding phenomenon occurs during the differential motion of the wheeled robot, the derivation process of the above kinematic equations needs to satisfy certain constraints [20], and the wheeled kinematic constraints:

$$\dot{x} \sin\theta - \dot{y} \cos\theta = 0 \tag{7}$$

2.5.2. Wheeled obstacle-crossing dynamics analysis

The mobile robot in the wheeled state studied in this paper is driven by two wheels, and the differential speeds of the motors of the left and right wheels are used to realize the robot's wheeled motions, such as left turn, right turn, and in situ rotation. When discussing its steering system dynamics, the dynamics model can be reasonably simplified.

Given $\sum F_x = 0$ in the horizontal plane, the driving force F_C of the wheel is related to the ground friction f and the acceleration:

$$M_x = f - F_c \tag{8}$$

Also since $\sum M = 0, J_\infty$ is the rotational inertia of the wheel and r is the radius of the wheel, it can be derived from the combined force moving around the wheel axis:

$$J_\omega \ddot{\theta} = T - H_f r \tag{9}$$

From the dynamic model of the stepper motor, the torque output to the wheel can be derived as:

$$T = I \frac{d_\omega}{d_t} = \frac{-k_m k_e}{R_m} \dot{\theta} + \frac{k_m}{R_m} V_a \tag{10}$$

where I is the current, k_m, $k_e$is the motor coefficient, R_m is the internal resistance of the motor, and V_a is the voltage to obtain the relationship between angle θ and friction:

$$M\ddot{x} = \frac{-k_m k_e}{R_m r} \dot{\theta} + \frac{k_m}{R_m} V_a - \frac{J_\omega}{r} \ddot{\theta} - F_c \tag{11}$$

Through the relationship between acceleration and angular acceleration, as well as velocity and angular velocity:

$$\begin{cases} \dot{\theta} r = \dot{x} \\ \ddot{\theta} r = \ddot{x} \end{cases} \tag{12}$$

This leads to the following equation:

$$\left(M + \frac{J_\omega}{r^2} \right) \ddot{x} = \frac{-k_m k_e}{R_m r^2} + \frac{k_m}{R_m r} V_a - F_c \tag{13}$$

https://doi.org/10.1017/S0263574725000499 Published online by Cambridge University Press

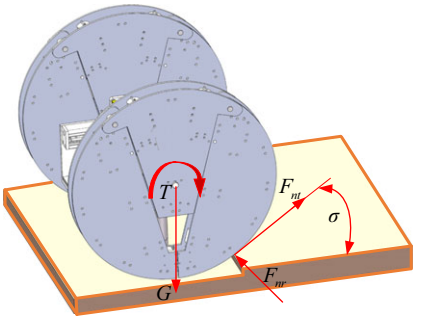


Figure 7. *Side view analysis of static transient forces when wheeling over small obstacles.*

To analyze the geometric relationship between the transformed wheel and the small obstacle protrusion, G is the gravitational force of the wheeled robot, as shown in Figure 7, F_{nr} and F_{nt} are the vertical and normal component forces on the contact surface, respectively, σ is the tangential angle between the wheeled robot and the small obstacle, and T is the torque supplied by the gear motor, and the static equations are established as follows.

$$M_1 = GL - T = 0 \tag{14}$$

$$F_y = F_{nr}\cos\sigma + F_{nt}\sin\sigma - G = 0 \tag{15}$$

Combining the above equations to solve for:

$$F_{nr} = \frac{G\tan\sigma}{\sin\sigma\tan\sigma + \cos\sigma} \tag{16}$$

$$F_{nt} = \frac{G}{\sin\sigma\tan\sigma + \cos\sigma} \tag{17}$$

2.5.3. Robot-legged motion analysis

The D-H parametric method, the spin-exponential product method, and the generalized coordinate method are often used in the kinematic modeling of legged robots [21], and the appropriate modeling method should be selected according to different mechanical structures when establishing the kinematic model of the system. In this paper, the quadruped robot performs obstacle-crossing, establishes the legged robot coordinate system, and adopts the modified D-H method to carry out positive kinematic analysis of the quadruped robot, and deduces the spatial position relationship between the telescopic foot end and the rotating joints, as shown in Figure 8 below, with the right front-end legged foot as an example, and the coordinate system is the body coordinate system.

The coordinate system is derived by simplifying the kinematic relations using the D-H parametric method with the following parameter list.

The left front leg and the right front leg have the same direction of joint rotation, so the parameter list is the same, and the DH parameters of the right front leg are listed in the Table 1 as an example.

(1) Forward kinematic analysis of robots

$$^{0}_{1}\boldsymbol{T} = \begin{bmatrix} \cos\gamma_1 & -\sin\gamma_1 & 0 & 0 \\ \sin\gamma_1 & \cos\gamma_1 & 0 & 0 \\ 0 & -1 & 1 & 0 \\ 0 & 0 & 0 & 1 \end{bmatrix} \tag{18}$$

$$^{1}_{2}\boldsymbol{T} = \begin{bmatrix} 1 & 0 & 0 & 0 \\ 0 & 0 & 1 & \varepsilon_1 \\ 0 & -1 & 0 & 0 \\ 0 & 0 & 0 & 1 \end{bmatrix} \tag{19}$$

https://doi.org/10.1017/S0263574725000499 Published online by Cambridge University Press

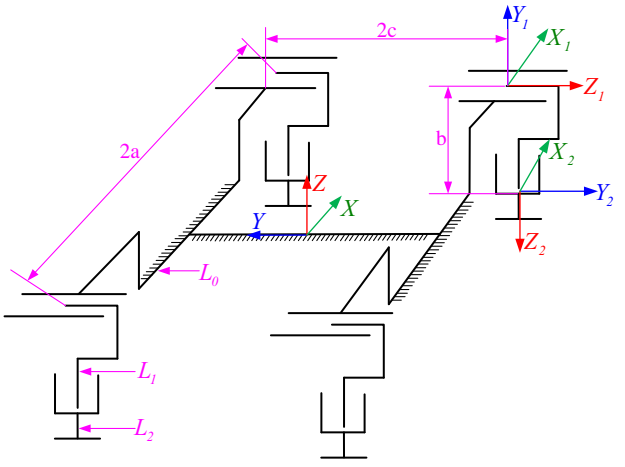


Figure 8. *Quadruped robot-legged state DH coordinate system.*

Table I. *DH parameters of the right front leg.*

	Connecting rod length		Rotation angle	Shifting		Joint angle	
Number	L_{i-1}	**Value/m**	α_{i-1}/°	**Variable**	**Value/m**	**Variable**	**Value/°**
1	L_1	a	90	–	c	γ_1	–
2	L_2	0	90	ε_1	–	–	0

$$ {}^{0}_{2}\boldsymbol{T}={}^{0}_{1}\boldsymbol{T}{}^{1}_{2}\boldsymbol{T}=\begin{bmatrix}\cos\gamma_1 & 0 & -\sin\gamma_1 & -\varepsilon\sin\gamma_1\\ \sin\gamma_1 & 0 & \cos\gamma_1 & \varepsilon\cos\gamma_1\\ 0 & -1 & 0 & 0\\ 0 & 0 & 0 & 1\end{bmatrix} \tag{20}$$

(2) Robot inverse kinematics analysis

The inverse kinematics in the articulated coordinate system {0} assumes that the chi-square transformation matrices are:

$$ {}^{1}_{2}\boldsymbol{T}=\begin{bmatrix}a_{11} & a_{12} & a_{13} & p_x\\ a_{21} & a_{22} & a_{23} & p_y\\ a_{31} & a_{32} & a_{33} & p_z\\ 0 & 0 & 0 & 1\end{bmatrix} \tag{21}$$

where p_x, p_y, p_z are the coordinate values of x, y, and z in the {0} coordinate system.

The expression for calculating each joint angle γ_{12} is:

$$\gamma_{12}=\arctan\left(\frac{p_x}{p_y}\right) \tag{22}$$

Translating this inverse kinematics to the body coordinate system {0}, let the

$$ {}^{0}_{2}\boldsymbol{T}=\begin{bmatrix}b_{11} & b_{12} & b_{13} & {}^{0}p_x\\ b_{21} & b_{22} & b_{23} & {}^{0}p_y\\ b_{31} & b_{32} & b_{33} & {}^{0}p_z\\ 0 & 0 & 0 & 1\end{bmatrix} \tag{23}$$

https://doi.org/10.1017/S0263574725000499 Published online by Cambridge University Press

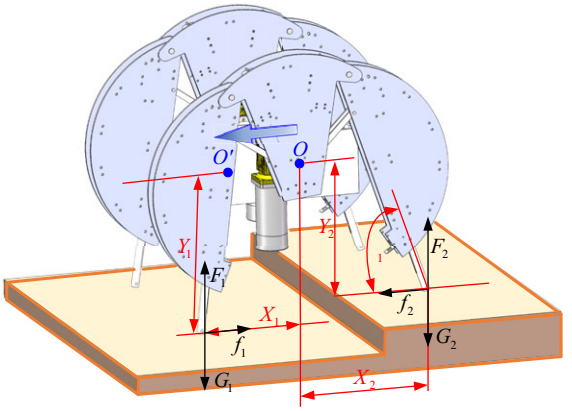


Figure 9. *Analysis of leg and foot forces for a legged robot climbing stairs.*

where ${}^0p_x$, ${}^0p_y$ and ${}^0p_z$ are the coordinate values of x, y, and z of the foot end in the {0} coordinate system, then

$$ {}^1_2\boldsymbol{T}=\begin{bmatrix} a_{11} & a_{12} & a_{13} & {}^0p_x-a \\ a_{21} & a_{22} & a_{23} & {}^0p_y-2c \\ a_{31} & a_{32} & a_{33} & {}^0p_z-2c \\ 0 & 0 & 0 & 1 \end{bmatrix} \tag{24} $$

$$ \begin{cases} p_x={}^0p_x-a \\ p_y={}^0p_y-2c \\ p_z={}^0p_z-2c \end{cases} \tag{25} $$

2.5.4. Analysis of the dynamics of legged overruns

Robot in the legged state is the primary consideration of the stability problem in the process of step, the stability of the robot is mainly determined by the stability margin, which is a key condition to ensure the stability of wheel-legged robots.

In this paper, the wheel-leg composite obstacle-crossing robot can be simplified as shown in Figure 9, where O point is the original body center of mass position point, when the legs and feet across the first step, the balance adjustment mechanism will be adjusted to the counterweight block relative to the back side of the O point, marked in the figure O' is that is adjusted for the body center of mass position point, through the analysis of the force in this plane, the relationship between the formula is as follows,

$$ \begin{cases} \sum F_X=0 \\ \sum F_Y=0 \\ \sum M=0 \end{cases} \tag{26} $$

$$ f_1-f_2=0 \tag{27} $$

$$ F_1+F_2-G_1-G_2=0 \tag{28} $$

$$ f_1Y_1+G_1X_1+F_2X_2-F_1X_1-G_2X_2-f_2Y_2=0 \tag{29} $$

Then the position O' of the adjusted center of gravity with respect to the geometric center point O is

$$ \begin{cases} O'_X=\frac{G_1X_1+F_2X_2-F_1X_1-G_2X_2}{G_1+F_2-F_1-G_2} \\ O'_Y=\frac{f_1Y_1-f_2Y_2}{f_1-f_2} \end{cases} \tag{30} $$

https://doi.org/10.1017/S0263574725000499 Published online by Cambridge University Press

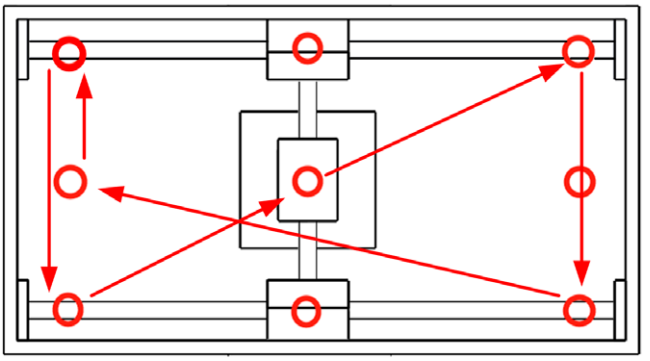


Figure 10. *Movement points of the counterweight position of the balance adjustment mechanism.*

When operating in the legged locomotion mode, the balance adjustment mechanism housed within the rectangular box collaborates with the robotic body to execute precise movements. Figure 10 illustrates a top-view schematic of the flat constant adjustment mechanism, wherein the actual width of the sliding components is disregarded for simplicity. The red-circled areas in the diagram denote the nine distinct motion zones for the counterweight within the rectangular box. In this study, the positional states of the counterweight in the balance adjustment mechanism are represented as point mappings. Real-time regulation of the center-of-mass adjustment mechanism is achieved through a rigorous analysis of the robotic dynamics during legged operation. As a result, it is possible to obtain a point map of the position of the counterweight block moving within the plane, as shown in Figure 10.

3. Robot virtual prototype simulation analysis

Dynamics simulation, as an important analysis tool for mobile robots, can simulate the motion characteristics of the physical prototype of the robot through the computer and guide the determination of robot design parameters and motion parameters. Under the premise of ensuring that the size and physical characteristics of each component remain unchanged, in order to facilitate simulation experiments, the simplified model of the robot is imported into the virtual simulation software Adams, and the simulation of wheeled walking is carried out to analyze the motion characteristics of the robot on the flat road and the road with small obstacles; quadrupedal walking and obstacle-crossing simulation is carried out to analyze the feasibility of the robot's obstacle-crossing gait and the performance of the robot in obstacle-crossing.

3.1 Wheel drive simulation

When the robot walks in wheeled mode, the transformed wheel-ground friction system is set to be 0.8, and the driving torque is 1.5 Nm, and the virtual simulation environment can be seen in Figure 11.

The Step function 0–5 s is used to gradually apply the drive torque to the deformed wheel to drive the robot to walk on a flat road without obstacles, and the curves of the motor drive torque and the robot walking speed are shown in Figure 12.

As can be seen from Figure 12, the robot's speed gradually increases under the action of the driving torque and stabilizes at a small fluctuation around 2.1 m/s after the 12th second. The main reason for this situation is that the center of mass of the transformed wheel is not on the axis of gyration, and the action of centrifugal force will affect the robot's stable traveling when it rolls.

Similarly, the driving torque is applied to drive the robot to walk on the road surface with small obstacles, setting the width of the gully 60 mm, the width of the camber 100 mm, the height of 20 mm, the motor driving torque and the robot walking speed curve is shown in Figure 13.

https://doi.org/10.1017/S0263574725000499 Published online by Cambridge University Press

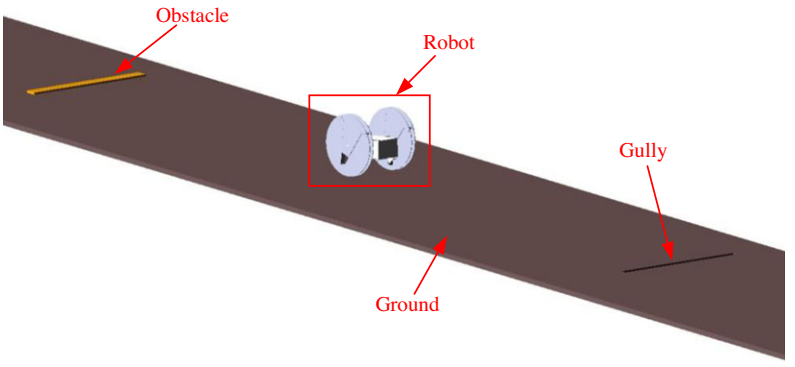


Figure 11. *Simulation that robot walking in the wheeled mode.*

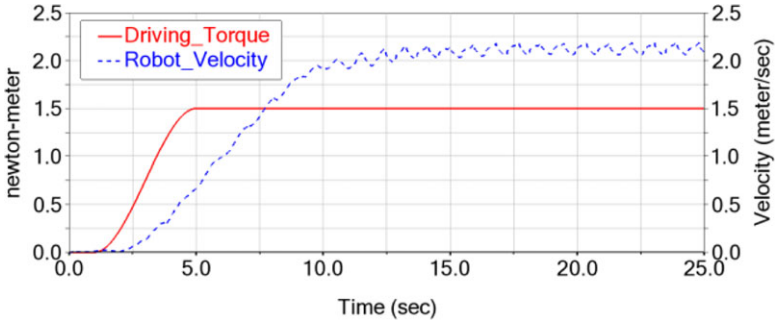


Figure 12. *Speed curve of robot walking on flat road in wheeled mode.*

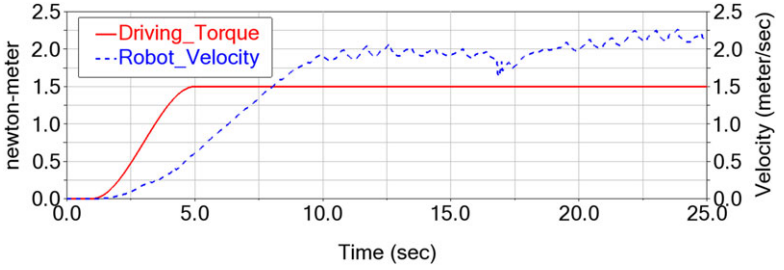


Figure 13. *Speed curve of robot walking on obstacle road in wheeled mode.*

During the robot's walk, it crosses a small gully at the 13th second and a raised platform at the 17th second, as can be seen from Figure 16, due to the large diameter of the transformed wheel, it is able to easily cross small obstacles, and the obstacles affect the robot's walking speed, and the robot resumes stable walking after the 22nd second, with a speed of approximately 2.1 m/s and accompanied by a small fluctuation.

3.2 Legged obstacle-crossing simulation

When the robot walks in legged mode, the friction system between the foot end and the ground is set to 1.0, and the virtual simulation experimental environment is constructed as shown in Figure 14.

Simulation experiments are carried out according to the obstacle-crossing process already planned, and the STEP function is used to drive the telescopic pusher moving vice, the leg pendulum rotating vice, and the balance-adjusting moving vice, so that the robot moves sequentially in accordance with the planned gait, as shown in Figure 15.

https://doi.org/10.1017/S0263574725000499 Published online by Cambridge University Press

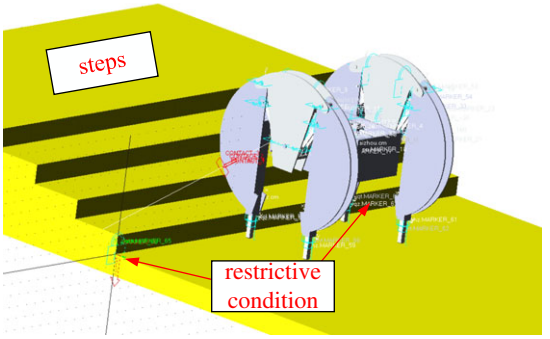


Figure 14. *Dynamic simulation model after adding constraints.*

In order to ensure the stability of the robot's foot walking, the center of mass adjustment mechanism needs to adjust the position of the counterweight block in time according to the robot's state, so that the robot's center of mass is always located within the range of the three supporting feet. The simulation process of robot motion is as follows: 0–2 s center of mass is adjusted to the right rear, 2–8 s left front leg steps up, 8–10 s center of mass is adjusted to the left rear, 10–16 s right front leg steps up, 16–18 s center of mass is adjusted to the front, 18–22 s the center of mass is shifted to the front as a whole, 22–24 s center of mass is adjusted to the right front, 24–30 s left rear leg steps forward, 30–32 s center of mass is adjusted to the left front, 32–38 s right rear leg is adjusted to the left front, 32–38 s center of mass is adjusted to the left front, 30–32 s center of mass is adjusted to the left front. Adjust the center of mass to the left front, 32–38 s step forward with the right hind leg, 38–40 s reset the center of mass to the center position and raise it up, then the robot steps up one step, repeats the above process and the robot can step over many steps.

Take the left front leg as an example, observe the relationship between the moving speed of the slider driving its swing and the swing angle and angular velocity, as shown in Figure 16, as well as the speed of the movement of the foot end of the left front leg and the support force, as shown in Figure 17.

The swing of each leg of the robot is driven by the slider through the transmission linkage, and the swing speed depends on the slider moving speed. It can be seen from Figure 16: the left front leg swings forward across the first step and the second step in 2–8 and 42–48 s, respectively, and the swing angle of the leg gradually increases; the robot center of mass moves forward in 18–22 and 58–60 s, and the left front leg swings backward, and the swing angle of the leg gradually decreases; the angular velocity curve of the left front leg follows the curve of the slider's moving speed, and the overall speed change is relatively smooth. The overall speed change is relatively smooth.

As can be seen in Figure 17, during 0–2 s when the center of mass of the robot is adjusted to the right rear, the force on the left forefoot gradually decreases to 0 N; during 2–8 s when the left foreleg steps onto the step, the velocity change of the left forefoot is relatively smooth; after 8–10 s when the center of mass is adjusted to the left rear, the force on the left foreleg is small, approximately 45 N; after 18–22 s when the center of mass of the robot is shifted forward, the force at the end of the foot increases to about 80 N, during which there are inconsistencies in the swing angle of the left and right forelegs. During this period, due to the inconsistency of the swing angle of the left and right front legs, the foot end slipped during the movement, and thus the speed change occurred; at the 30th second, the rear leg had already stepped forward to support the weight of the robot, and the force on the foot end of the left front leg decreased; after the 40th second, there was the second action cycle, which was similar to the first action cycle mentioned above, During this period, the robot's center of mass adjustment and leg and foot retraction mechanisms are still in action, resulting in a small fluctuation of force on the end of the foot that is in substantial contact with the ground.

The multi-periodic trend of the whole machine's center of mass displacement and moving velocity in the vertical direction of the ground as the robot climbs the steps is shown in Figure 18.

https://doi.org/10.1017/S0263574725000499 Published online by Cambridge University Press

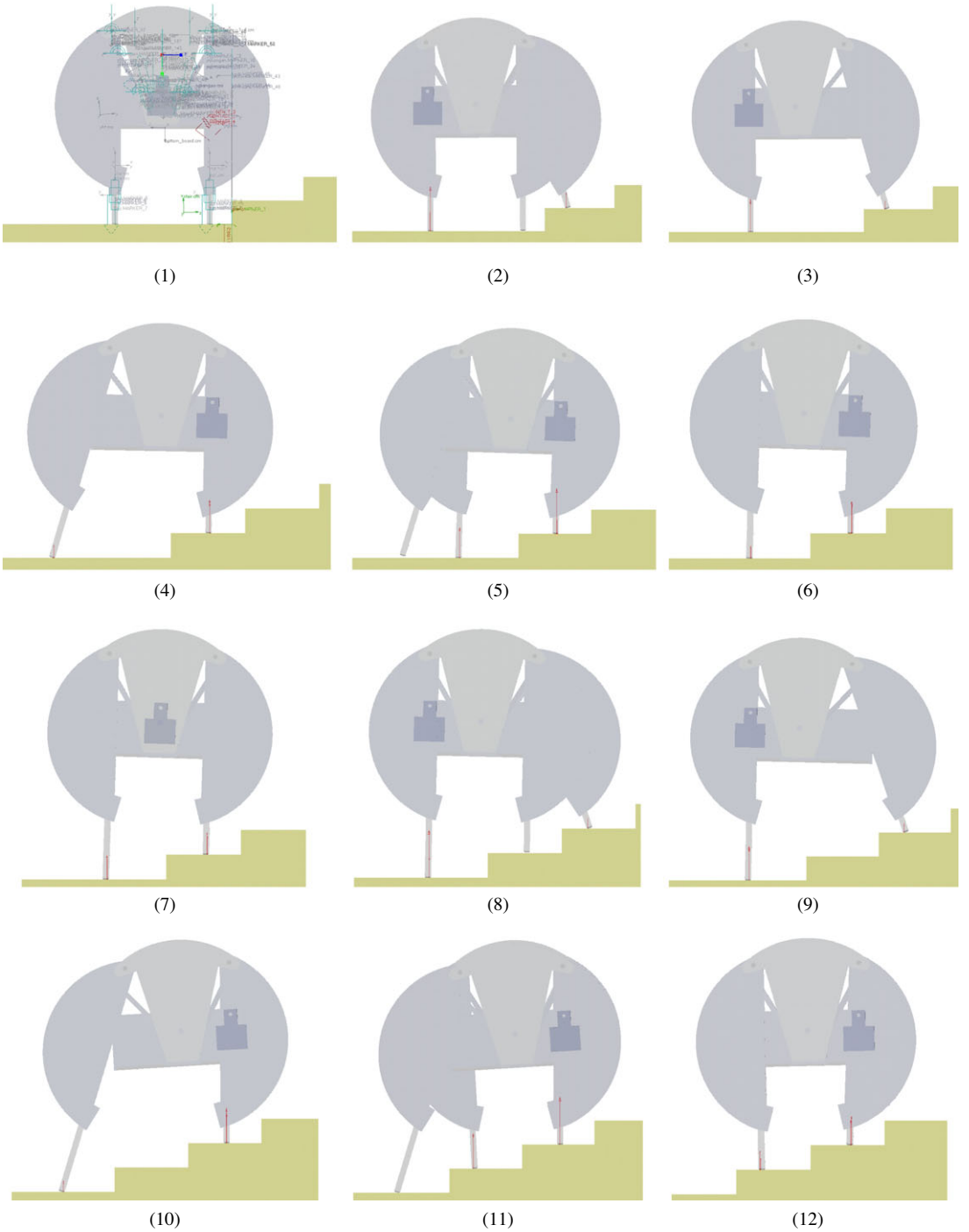


Figure 15. *Gait simulation that robot crossing stair steps.*

In the 0–18 s time period, the robot's two front legs step onto the first step, and the robot's center of mass only adjusts its position in the horizontal plane, so there is no change in the direction of the center of mass velocity and height; in the 18–22 s time period, the robot's front leg swings backward and the back leg swings forward, which causes the robot's center of mass to move forward as a whole and raise,

https://doi.org/10.1017/S0263574725000499 Published online by Cambridge University Press

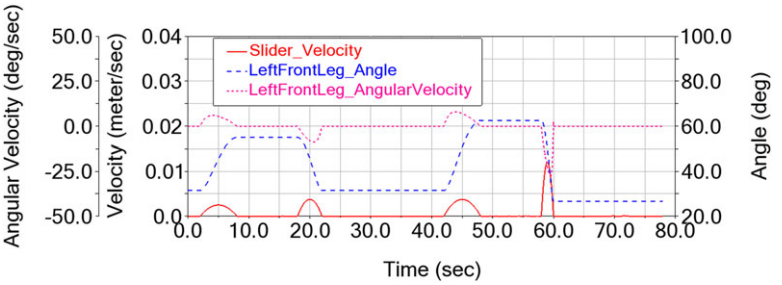


Figure 16. *Slider velocity and swinging angle and angular velocity curves of the left front leg.*

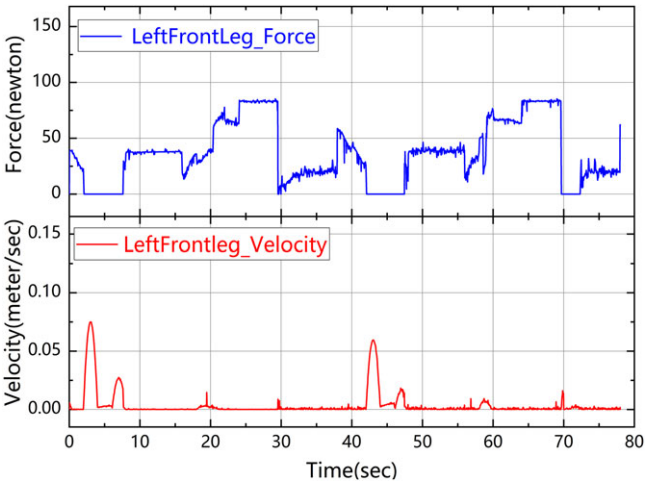


Figure 17. *Velocity and force curves of the left front leg.*

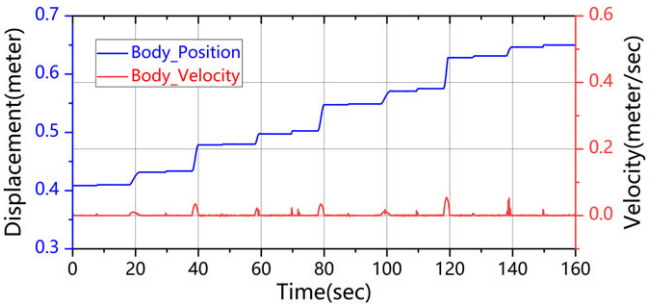


Figure 18. *Displacement and velocity curves of robot center of mass.*

so there is a change in the velocity of the center of mass and an increase in the height. During the 22–38 s time period, the robot's two rear legs step forward and the robot's center of mass velocity and height direction do not change. During the 38–40 s time period, the robot's four legs extend at the same time, which causes the robot's center of mass to raise, and prepares for the front leg to step onto the second step.

The forces on the foot ends of the four legs during the robot's obstacle crossing are shown in Figure 19.

Robot four feet alternately step walking, four feet force change rule is similar, the end of the foot lift step when the force is 0 N, support the robot weight when the force size and robot center of gravity position; four feet combined force is equal to the robot's gravity, about 200 N. Due to the robot end of the foot contact with the ground in the simulation environment for the rigid contact, so the end of the foot force and force fluctuation is larger.

https://doi.org/10.1017/S0263574725000499 Published online by Cambridge University Press

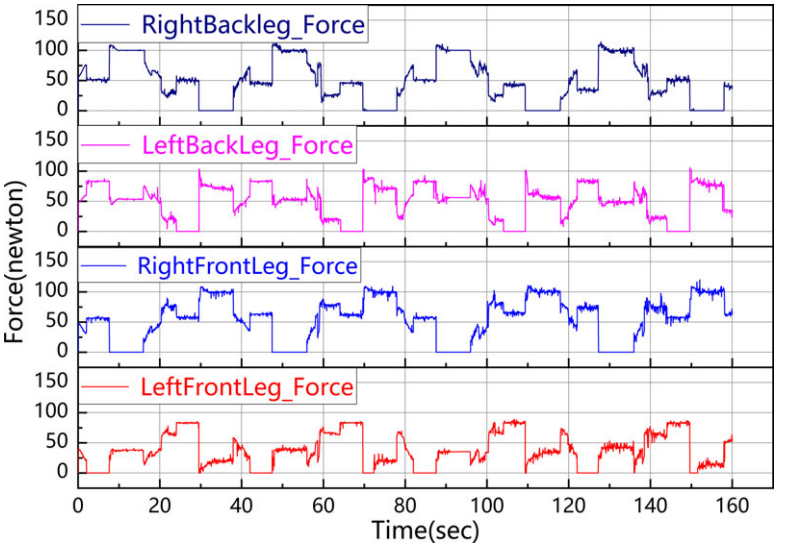


Figure 19. *Force curves of the four legs.*



Figure 20. *The prototype composite robot in wheeled state.*

4. Robot prototype experiments

In the experimental phase, several instances were observed where the T-shaped area at the screw slider reached its limit position, coupled with a lag error in motor response time. This combination of factors led to the motor output coupling reaching its operational limits, ultimately resulting in phenomena such as load-induced fracture failures. To address this issue, travel switches were installed at both ends of the screw within the prototype. These switches are triggered when the slider approaches its positional limits, generating a stop signal that immediately halts the operation of the DC motor.

After modeling optimization, parts drawing and physical assembly of the prototype, the equal scale solid prototype is shown in Figures 20 and 21 below.

Based on the gait planning for robot-legged obstacle crossing, a prototype experiment for crossing steps was conducted, as shown in Figure 22.

https://doi.org/10.1017/S0263574725000499 Published online by Cambridge University Press

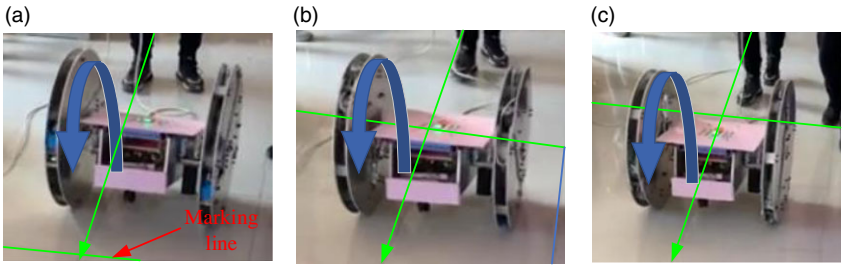


Figure 21. *Screenshot of wheeled robot rolling video.*

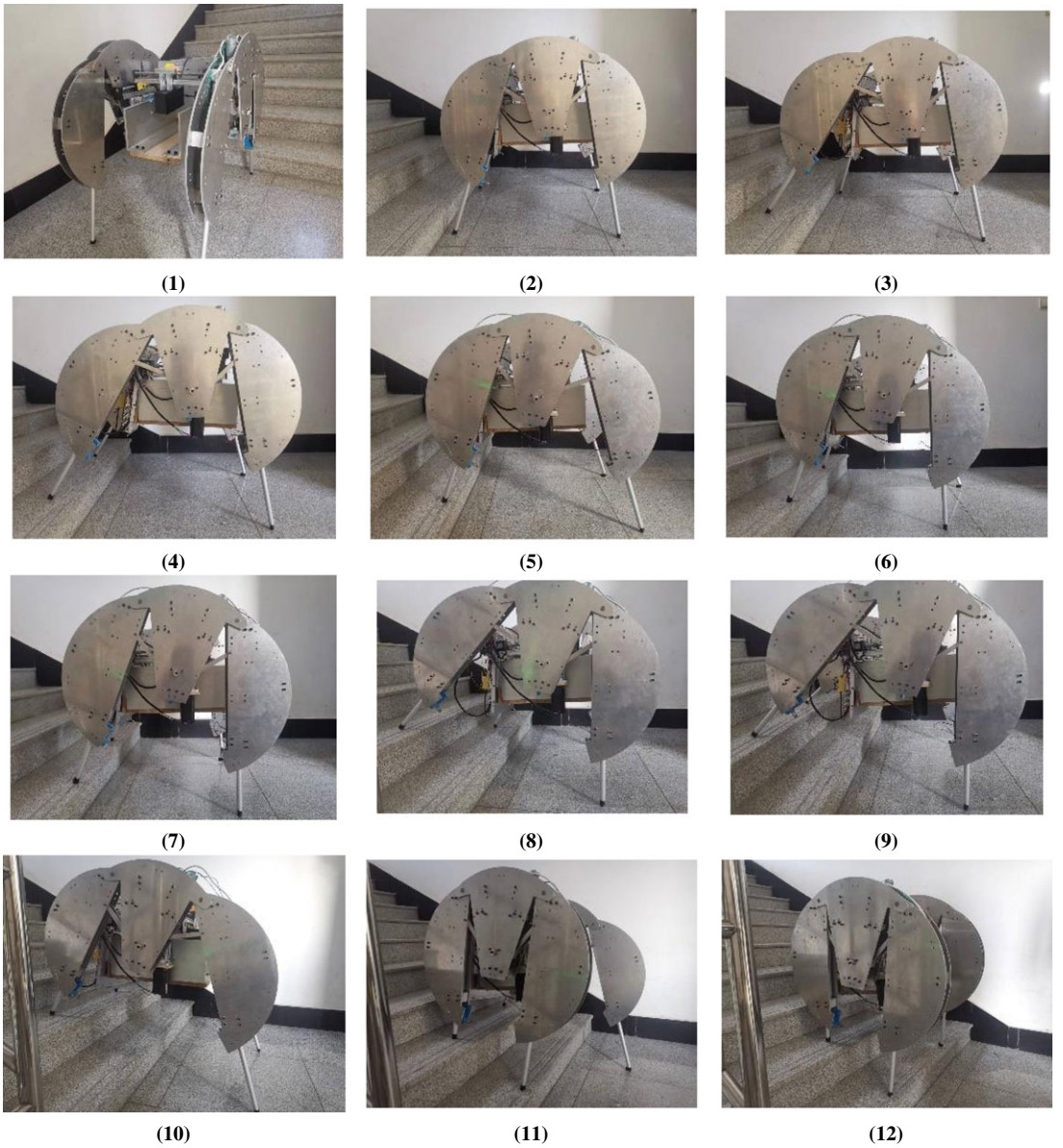


Figure 22. *Prototype experiment that robot climbing the stairs in the legged mode.*

https://doi.org/10.1017/S0263574725000499 Published online by Cambridge University Press

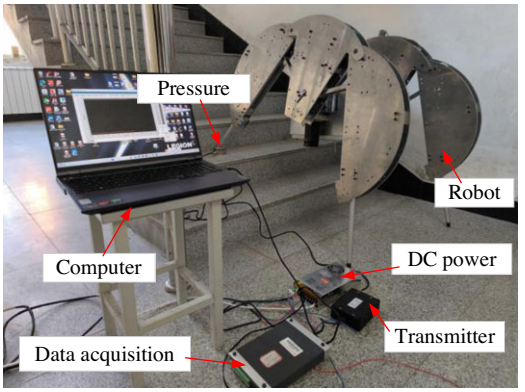


Figure 23. *Experimental environment for robot foot-ground pressure test.*

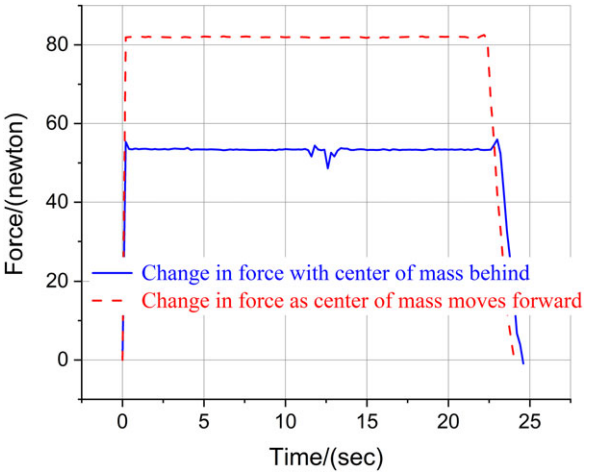


Figure 24. *Robot foot-ground pressure change curve.*

In the experimental process of a robot prototype climbing stairs, the robot exhibited improved stair-climbing smoothness, with relatively consistent swing motions of its four legs. However, the support end of the foot often experienced noticeable sliding during contact with the ground. This issue primarily stems from the absence of specialized anti-slip foot components at the terminal end of the telescopic actuator. The interaction between the rigid terminal end of the telescopic actuator and the ground surface results in a low coefficient of friction, ultimately leading to insufficient frictional forces.

In order to examine the effect of the robot's movements during climbing on the magnitude of the load applied to the foot end of the telescopic mechanism, a foot end pressure variation test experiment was carried out, as shown in Figure 23.

Sequentially, the foot end of the left front leg of the robot was tested with different loads at different positions of the center of mass adjustment mechanism, as shown in Figure 24. The experimental data show that when the robot's center of mass is at the rear of the body, the actual force on the foot end is measured to be about 53 N. When the robot's center of mass is at the front of the body, the actual force on the foot end is measured to be about 81 N. It is analyzed that the actual measurements are bigger than the simulation data, and the overall trend is the same. Therefore, the actual robot load is greater than the value set in the simulation. In Figure 24, both the blue and red curves exhibit transient elevations at both the initial and final segments. These elevations arise from transient pressure variations at the foot end, which are attributed to the inertial forces generated when the center-of-mass adjusting mechanism ceases its motion abruptly upon reaching the designated position. Specifically, the elevated segment in

https://doi.org/10.1017/S0263574725000499 Published online by Cambridge University Press

the blue curve is attributable to an anomalous fluctuation in the data, stemming from the sliding of the robot's foot on the smooth floor step during the acquisition of the foot force data.

5. Conclusion

(1) A single deformed wheel is divided into a bracket and two legs by the method of three-segment segmentation circle, and each leg is equipped with a leg length adjusting mechanism and a leg pendulum driving mechanism, which proves the feasibility of the deformed wheel structural design and the mutual transformation of the wheel shape and leg shape through theoretical analyses, numerical calculations, and simulation and experiment of the robot's motion.

(2) A two-wheeled quadruped robot is constructed by using the deformed wheel, and the robot's legged walking gait over obstacles is planned, and the effectiveness of the robot's wheeled and legged walking is verified by using virtual simulation and prototype experiments to prove the feasibility of the mechanical structure of the two-wheeled quadruped robot.

(3) The prototype was subjected to a foot-end pressure test experiment, and the results of the prototype experiment were basically consistent with the simulation results, which proved the feasibility of the foot-ground contact support body.

(4) The robot virtual simulation experiments show that due to the eccentricity of the center of mass of the deformed wheel, the speed fluctuation of the robot is large when it is rolling, which affects the stability of the robot, and the robot's stability is in the critical steady state when it is walking with its feet. In summary, the next step of the work requires innovative design of the robot structure, transformed wheel counterweight adjustment device, and robot center of mass adjustment mechanism.

Author contributions. Xin Mei and Yongle Wei designed the study. Xingyuan Zhang and Chenguang Guo provided the supervision.

Financial support. This work was supported by Basic Scientific Research Project of the Educational Department of Liaoning Province (Grant No.LJ2020JCL024) and Research start-up funding project of QuZhou University (Grant No. BSYJ202216).

Competing interests. The authors declare that no conflicts of interest exist.

Ethical standards. Not applicable.

References

[1] T. L. Yang, *Topology Design of Robot Mechanisms* (Science Press, Beijing, 2012).
[2] X. B. Liu, *Design and Research of Wheel-Leg Composite Mine Rescue Robot* (Shandong University of Science and Technology, 2020). doi:10.27275/d.cnki.gsdku.2020.001808
[3] K. Xu, S. K. Wang, B. K. Yue, J. Z. Wang, H. Peng, D. C. Liu, Z. Chen and M. Shi, "Adaptive impedance control with variable target stiffness for wheel-legged robot on complex unknown terrain," *Mechatronics* **69**(5), 102388 (2020).
[4] Q. Q. Zhang, Y. Z. Li, Y. A. Yao and R. M. Li, "Design and locomotivity analysis of a novel deformable two-wheel-like mobile mechanism," *Ind. Robot Int. J. Rob. Res. Appl.* **47**(3), 369–380 (2020).
[5] Y. C. Ma and F. J. Lyu, "Design of A Wheel-Legged Stair Climbing Robot," **In:** 2021 7th International Conference on Control, Automation and Robotics (ICCAR) (IEEE, 2021) pp. 146–150.
[6] Y. M. Song, C. Y. Hao and W. L. Yue, "Kinematic analysis and design of a new deformed wheel-legged mobile robot," *J. Tianjin Univ. (Nat. Sci. Eng. Technol.)* **55**(02), 111–121 (2022).
[7] M. Bjelonic, R. Grandia, O. Harley, C. Galliard, S. Zimmermann and M. Hutter, "Whole-Body MPC and Online Gait Sequence Generation for Wheeled-Legged Robots," **In:** 2021 IEEE/RSJ International Conference on Intelligent Robots and Systems (IROS) (IEEE, 2021) pp. 8388–8395.
[8] N. Mao, J. Chen, E. Spyrakos-Papastavridis and J. S. Dai, "Dynamic modeling of wheeled biped robot and controller design for reducing chassis tilt angle," *Robotica* **42**(8), 2713–2741 (2024). doi:10.1017/S0263574724001061.
[9] E. Ottaviano and P. Rea, "Design and operation of a 2-DOF leg-wheel hybrid robot," *Robotica* **31**(8), 1319–1325 (2013). doi:10.1017/S0263574713000556.
[10] L. Z. Zhang, F. S. Zha, W. Guo, C. Chen, L. N. Sun and P. F. Wang, "Heavy-duty hexapod robot sideline tipping judgment and recovery," *Robotica* **42**(5), 1403–1419 (2024). doi:10.1017/S0263574724000274.

https://doi.org/10.1017/S0263574725000499 Published online by Cambridge University Press

[11] L. F. Liang, Y. Q. Xu, H. Liang and L. Yu, "System design and control of the sphere-wheel-legged robot," *Robotica* **42**(10), 3363–3379 (2024).
[12] J. D. Cao, J. Zhang, T. Wang, J. H. Meng, S. L. Li and M. Li, "Mechanism design and dynamic switching modal control of the wheel-legged separation quadruped robot," *Robotica* **42**(3), 660–683 (2024).
[13] Y. S. Kim, G. P. Jung, H. Kim, K. Cho and C. Chu, "Wheel transformer: A wheel-leg hybrid robot with passive transformable wheels," *IEEE Trans. Rob.* **30**(6), 1487–1498 (2014).
[14] Y. Yang, R. Z. Zhang, C. H. Guang and Y. Wang, "A multi-segment deformed wheel for mobile robots," *J. Beijing Univ. Aeronaut. Astronaut.* **44**(08), 1712–1719 (2018).
[15] S. Soyguder and W. Boles, "SLEGS robot: Development and design of a novel flexible and self-reconfigurable robot leg," *Ind. Robot Int. J.* **44**(3), 377–391 (2017).
[16] K. Tadakuma, R. Tadakuma, A. Maruyama, E. Rohmer, K. Nagatani and K. Yoshida, "Mechanical Design of the Wheel-Leg Hybrid Mobile Robot to Realize a Large Wheel Diameter," **In:** IEEE/RSJ International Conference on Intelligent Robots and Systems (IEEE, 2010) pp. 3358–3365.
[17] X. D. Chen, *Motion Planning and Control of Multi-Legged Walking Robots* (Huazhong University of Science and Technology Press, 2006).
[18] H. Y. Tang, J. W. Zhang, L. Q. Pan and D. Zhang, "Optimum design for a new reconfigurable two-wheeled self-balancing robot based on virtual equivalent parallel mechanism," *J. Mech. Des.* **145**(5), 053302 (2023).
[19] F. Grasser, A. D'arrigo, S. Colombi and A. C. Rufer, "JOE: A mobile, inverted pendulum," *IEEE Trans. Ind. Electron.* **49**(1), 107–114 (2002).
[20] J. H. Dai, *Research on Localisation and Map Building Algorithm of Coal Mine Rescue Robot with High Power Intrinsically Safe Drive* (Chongqing University, 2019). doi:10.27670/d.cnki.gcqdu.2019.002641
[21] P. L. Yang, *Reconfiguration Motion Analysis and Stability Control of Wheel-Legged Varicellular Robot during Parking and Steering* (Hefei University of Technology, 2021). doi:10.27101/d.cnki.ghfgu.2021.002011

Cite this article: X. Mei, Y. Wei, C. Guo and X. Zhang (2025). "Experimental research of wheel-legged robot crossing obstacles", Robotica **43**, 2459–2479. https://doi.org/10.1017/S0263574725000499

https://doi.org/10.1017/S0263574725000499 Published online by Cambridge University Press